AIAA-93-0767
A Fast Multigrid Method for Solving Incompressible Hydrodynamic Problems with Free Surfaces

J. Farmer, L. Martinelli and A. Jameson
Princeton University
Princeton, NJ

31st Aerospace Sciences Meeting & Exhibit
January 11-14, 1993 / Reno, NV

A Fast Multigrid Method For Solving Incompressible Hydrodynamic Problems With Free Surfaces

J. Farmer, L. Martinelli,
A. Jameson
Department of Mechanical and Aerospace Engineering
Princeton University
Princeton, NJ. 08544

Acknowledgement

Partial support for this work was provided through ONR Grant N00014-89-J-1366 and DARPA Grant N00014-89-J-0759. This support is gratefully acknowledged by the authors. [1]

1 Introduction

Of great interest over the last two decades has been the modeling of aircraft flying in the Mach number range of approximately 0.80 to 0.85. This speed range typically results in the most favorable cruise performance, whence it is desirable to accurately predict the stability and power requirements over this range. However, this speed range also results in the complex and *a priori* unknown supersonic region over the wings and other surfaces of the fuselage. The necessity of accurately predicting this complex flow field has led to much progress in the numerical solution of compressible air flows about arbitrary bodies in recent years [1]. Unfortunately, the successful methods for compressible flow simulation are not normally applicable to flows with low Mach number. Specifically, in the limit of truly incompressible flow, or zero Mach number, alternate methods must be used to compute the flow field. Many of these methods have certain unfavorable drawbacks. Thus the purpose of the work described herein is to present a method, for treating truly incompressible flows, that retains the favorable characteristics of the recently developed compressible flow codes. The free surface ship wave problem is presented to show the method's versatility to problems other than incompressible low speed air flows. This problem retains many of the complexities associated with aircraft modeling, namely predicting the fluid flow about arbitrary fuselage/wing combinations (or hull/keel for hydrodynamic case). However, it is further complicated since it requires finding the *a priori* unknown free surface location as part of the solution. The main direction of the present work is to accurately compute the free surface location, additional work will focus on hull/keel junctures inclined at realistic attack angles.

The fundamental problem in working with incompressible flows, even flows without the complication of a free surface, is the loss of an evolution equation for density. Since density is constant, the time derivative is zero and thus a time independent velocity constraint must be imposed on the momentum equations. In addition, if one were to examine the eigenvalues resulting from the system of conventional hyperbolic Euler equations for compressible flows, one would find, in the limit of incompressible flow, the waves to travel in all directions, infinitely fast. This is so based on physical grounds as well since incompressible flows exhibit infinite sound speeds. Thus, the well established methods for computing compressible flows may not be used for the incompressible case.

The method used by Hino [2] is characteristic of the general approach to solving incompressible flow problems (see also the recent works of Miy-

ata et al [3] and Tahara et al [4]). This method involves taking the divergence of the momentum equation and iterating, implicitly at each global time step, the pressure and velocity fields such that continuity is satisfied. The method tends to be expensive due to its implicit nature and complicated due to taking the divergence of momentum equations in a curvilinear coordinate system.

In this work, an approach referred to as *artificial compressibility* is adopted. The approach was proposed by Chorin [5] in 1967 as a method to solve viscous flows. Since then, Rizzi and Eriksson [6] have applied it to rotational inviscid flow, Dreyer [7] has applied it to low speed two dimensional airfoils and Kodama [8] has applied it to ship hull forms and propellers with rigid free surface. In addition, Turkel [9] has investigated more sophisticated preconditioners than the original idea proposed by Chorin. The basic idea behind artificial compressibility is to introduce a pseudotemporal equation for the pressure through the continuity equation. This approach removes the troublesome sound waves associated with compressible flow formulations with small Mach number; which is zero in the limit of truly incompressible flow. The system waves, or eigenvalues, are now replaced with a different "artificial" set that renders the new set of equations well conditioned for numerical computation. This arises through the preconditioning matrix which is the basis for artificial compressibility. When combined with multigrid acceleration procedures [10, 11, 12] it proves to be particularly effective. Converged solutions of incompressible flows over three dimensional isolated wings are obtained in 25 - 50 cycles.

The general objective of this work is the development of a more efficient method to predict free surface wave phenomena. A new method based on a coupling between an artificial compressibility, multigrid Euler scheme and a free surface formulation is presented [13] and comparisons made with available experimental data [14]. The new method is efficient and allows for straight forward extension to include viscous terms associated with Navier-Stokes equations and a turbulence model. This extension will facilitate the simulation of not only free surface wave patterns, but the frictional and any induced drag components as well.

2 Mathematical Model

Figure 1 shows the reference frame and ship location with respect to the same used in this work. A right-handed coordinate system $Oxyz$, with the origin fixed at midship on the mean free surface is established. The z direction is positive upwards, y is positive towards the starboard side and x is positive in the aft direction. The free stream velocity vector is parallel to the x axis and points in the same direction. The ship hull pierces the uniform flow and is held fixed in place, ie. the ship is not allowed to sink (translate in z direction) or trim (rotate in $x-z$ plane).

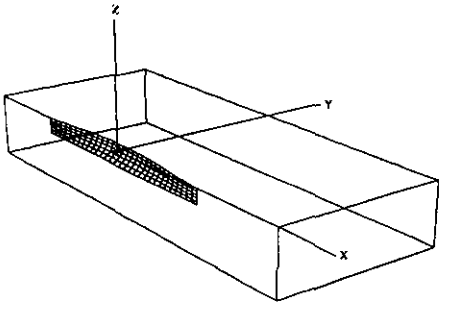

Figure 1: Reference Frame and Ship Location

For a nonviscous incompressible fluid moving under the influence of gravity the continuity and Euler equations may be put in the form [2],

$$u_x + v_y + w_z = 0, \tag{1}$$

$$u_t + uu_x + vu_y + wu_z = -\psi_x,$$

$$v_t + uv_x + vv_y + wv_z = -\psi_y,$$

$$w_t + uw_x + vw_y + ww_z = -\psi_z.$$

Here, $u = u(x,y,z,t)$, $v = v(x,y,z,t)$ and $w = w(x,y,z,t)$ are total velocity components in the x,y,z directions; all lengths and velocities are nondimensionalized by the ship length L and free stream velocity U, respectively. The pressure ψ is the static pressure p with the hydrostatic component extracted. This may be expressed as $\psi = p + zFr^{-2}$ where $Fr = \frac{U}{\sqrt{gL}}$ is the Froude number; pressure is nondimensionalized by ρU^2. This set of equations shall be solved subject to the following boundary conditions.

When the effects of surface tension and viscosity are neglected, the boundary condition on the free surface consists of two equations. The first, the dynamic condition, states simply that the pressure acting on the free surface is constant, or equal to atmospheric as is for normal ship waves. The second, the kinematic condition, states that the free surface is a material surface, or in other words, once a fluid particle is on the free surface, it forever remains on the surface. The dynamic and kinematic boundary conditions may be expressed as follows

$$p = constant,$$

$$\frac{d\beta}{dt} = w = \beta_t + u\beta_x + v\beta_y, \qquad (2)$$

where $z = \beta(x, y, t)$ is the free surface location. Equation 2 only permits solutions where β is single valued and thus does not permit bow wave breaking phenomena characteristic of cruiser type hulls. These types of breaking waves are difficult to formulate numerically and are not considered in this work.

The remaining boundary conditions consist of the ship hull, the boundaries which comprise the symmetry portions of the meridian plane and the far field conditions of the computational domain. On the ship hull the condition is that of impermeability and is stated simply by

$$\mathbf{q} \cdot \mathbf{n} = un_x + vn_y + wn_z = 0,$$

where the normal vector $\mathbf{n}$ may be assumed to point into the flow. On the symmetry plane (that portion of the (x,z) plane excluding the ship hull) derivatives in the y direction as well as the v component of velocity are set to zero. The upstream plane has $u = U$ and $\psi = 0$ ($p = zFr^{-2}$); all other components set to zero. Similar conditions hold on the bottom plane which is assumed to represent infinitely deep water where no disturbances are felt. The starboard plane uses one sided differences to update flow variables rather than simply setting them to free stream values. A radiation condition must be imposed on the outflow domain to allow the wave disturbance to pass out of the computational domain. Although fairly sophisticated devices may be constructed to facilitate the radiation condition [15], in this work extrapolations have been found to be sufficient for reasons discussed later on.

3 Numerical Solution

This section presents some details of the procedure used for the solution of the incompressible bulk flow Euler formulation in conjunction with a free surface. Basically, the method involves the artificial compressibility, finite volume method (FVM) for the bulk flow variables (u, v, w and ψ), coupled to a finite difference method for the free surface evolution variables (β and ψ). Alternative cell-centered and cell-vertex formulations may be used in finite volume schemes [10]. A cell-vertex formulation was preferred in this work because values of the flow variables are needed on the boundary to implement the free surface boundary condition. The bulk flow is solved subject to Dirichlet conditions for the free surface pressure, followed by a free surface update via the bulk flow solution (ie. Dirichlet conditions on velocities in equation 2). Each formulation is explicit and uses local time stepping. Both multigrid and residual averaging techniques are used in the bulk flow to accelerate convergence.

3.1 Bulk Flow Solution

Following Chorin [5] and more recently Dreyer [7], the governing set of incompressible flow equations may be written in vector form as,

$$\frac{\partial \mathbf{w}}{\partial t^*} + \mathbf{P}\left(\frac{\partial \mathbf{f}}{\partial x} + \frac{\partial \mathbf{g}}{\partial y} + \frac{\partial \mathbf{h}}{\partial z}\right) = 0, \qquad (3)$$

where the vector of dependent variables, $\mathbf{w}$ and flux vectors, $\mathbf{f}, \mathbf{g}$ and $\mathbf{h}$ are given by

$$\begin{aligned} \mathbf{w} &= [\psi,\ u,\ v,\ w]^T, \\ \mathbf{f} &= [u,\ u^2 + \psi,\ uv,\ uw]^T, \\ \mathbf{g} &= [v,\ vu,\ v^2 + \psi,\ vw]^T, \\ \mathbf{h} &= [w,\ wu,\ wv,\ w^2 + \psi]^T. \end{aligned}$$

The preconditioning matrix $\mathbf{P}$ is given by,

$$\mathbf{P} = \begin{bmatrix} \Gamma^2 & 0 & 0 & 0 \\ 0 & 1 & 0 & 0 \\ 0 & 0 & 1 & 0 \\ 0 & 0 & 0 & 1 \end{bmatrix},$$

where Γ^2 is called the "artificial compressibility" due to the analogy that may be drawn between the above equations and the equations of motion of a compressible fluid whose equation of state is given by,

$$p = \Gamma^2 \rho.$$

Thus, ρ is an artificial density and Γ may be referred to as an artificial sound speed. Note that although the equations for momentum are in compressible flow form, when temporal derivatives tend to zero, the set of equations satisfy precisely the incompressible Euler equations. This is a key point since it indicates how the correct pressure may be established using the "construct" of artificial compressibility. The preconditioning matrix $\mathbf{P}$ may be viewed as a device to create a well posed system of hyperbolic equations that are to be integrated to steady state along lines similar to the well established compressible flow FVM formulation [12]. In addition, the artificial compressibility parameter may be viewed as a relaxation parameter for the pressure iteration. Note also that temporal derivatives are now denoted by t^* to indicate pseudo time; the artificial compressibility, as formulated in the present work, destroys time accuracy.

To demonstrate the effect of the preconditioning matrix on the above set of equations and to establish the hyperbolicity of the set, equation 3 may be written in quasilinear form to determine the eigenvalues [6]. The eigenvalues are found to be,

$$\lambda_1 = U, \;\; \lambda_2 = U, \;\; \lambda_3 = U + a, \;\; \lambda_4 = U - a$$

where

$$U = u\xi + v\eta + w\zeta$$

and

$$a^2 = U^2 + \Gamma^2(\xi^2 + \eta^2 + \zeta^2).$$

The terms ξ, η and ζ represent the slopes of the characteristic system waves, are arbitrary and defined (ie. $-\infty \leq \xi, \eta, \zeta \leq +\infty$). Since the eigenvalues are clearly real for any value of ξ, η and ζ, the system of equations 3 is guaranteed to be hyperbolic.

What is most important to note from the above result is that the choice of Γ is crucial in determining convergence and stability properties of the numerical scheme. Typically the convergence rate of the scheme is dictated by the slowest system waves and the stability of the scheme by the fastest. Thus it is seen, that in the limit of large Γ the difference in wave speeds can be large. Although this would presumably lead to a more accurate solution through the "penalty effect" in the pressure equation, very small time steps would be required to ensure stability. Conversely, for small Γ, the difference in the maximum and minimum wave speeds may be significantly reduced, but at the expense of accuracy. Thus a compromise between the extremes is required. Following the work of Dreyer, the choice for Γ was taken to be,

$$\Gamma^2 = C(u^2 + v^2 + w^2)$$

where C is a constant of order unity. Whence, in regions of high velocity, where low pressure and suction occur, Γ is large to better enforce accuracy. In regions of lower velocity Γ is correspondingly reduced.

Another important point regarding the choice of Γ concerns the outflow boundary condition, or radiation condition. In this work, approximate nonreflecting boundary conditions were developed based on analogous hyperbolic computations for supersonic flow. As is well known, if it can be demonstrated that all system eigenvalues are not only real, but positive as well, then downstream or outflow boundary points may be extrapolated from the interior upstream. Examination of the eigenvalues presented earlier suggest that this can never be so, but, the condition can be approached by a judicious choice of Γ. If Γ is large, then extrapolation will not work because a downstream dependence exists as well as the upstream dependence. As Γ is reduced, the upstream dependence becomes more pronounced and the downstream becomes less. As it turns out, by taking Γ as outlined before, the upstream dependence is sufficiently dominate to allow extrapolation. Whence, all outflow variables are updated using zero gradient extrapolation.

Following the general procedures for FVM the governing equations may be integrated over an arbitrary volume Ω. Application of the divergence theorem on the flux term integral yields,

$$\frac{\partial}{\partial t^*}\int_\Omega \mathbf{w} d\Omega + \mathbf{P}\int_{\partial\Omega}(\mathbf{f}dS_x + \mathbf{g}dS_y + \mathbf{h}dS_z) = 0,$$

where S_x, S_y and S_z are the directed areas in the x, y and z directions, respectively. The computational domain is divided into hexahedral cells. Application of FVM to each of the computational cells results in the following system of ordinary differential equations,

$$\frac{d}{dt^*}(V_{ijk}\mathbf{w}) + Q_{ijk} = 0.$$

Here, the volume V_{ijk} is given by the summation of the eight cells surrounding node i,j,k and

$Q_{ijk}(\mathbf{w})$ is defined as

$$Q_{ijk}(\mathbf{w}) = \sum_{k=1}^{n} (\mathbf{f}S_x + \mathbf{g}S_y + \mathbf{h}S_z)_k$$

where the summation is over the n faces surrounding V_{ijk}.

In practice, the grid mesh is body fitted and hence non-Cartesian. A curvilinear transformation, defined by

$$\xi = \xi(x,y,z), \quad \eta = \eta(x,y,z), \quad \zeta = \zeta(x,y,z),$$

is incorporated leading to a modified approach to the flux evaluation in the new, transformed space. The new approach becomes

$$Q_{ijk} = \frac{\partial \tilde{\mathbf{f}}}{\partial \xi} + \frac{\partial \tilde{\mathbf{g}}}{\partial \eta} + \frac{\partial \tilde{\mathbf{h}}}{\partial \zeta},$$

where

$$\tilde{\mathbf{f}} = J\{\tilde{u}, u\tilde{u} + \xi_x\psi, v\tilde{u} + \xi_y\psi, w\tilde{u} + \xi_z\psi\}^T$$

$$\tilde{\mathbf{g}} = J\{\tilde{v}, u\tilde{v} + \eta_x\psi, v\tilde{v} + \eta_y\psi, w\tilde{v} + \eta_z\psi\}^T$$

$$\tilde{\mathbf{h}} = J\{\tilde{w}, u\tilde{w} + \zeta_x\psi, v\tilde{w} + \zeta_y\psi, w\tilde{w} + \zeta_z\psi\}^T.$$

The contravariant velocity components $\tilde{u}, \tilde{v}$ and $\tilde{w}$ are given by

$$\tilde{u} = u\xi_x + v\xi_y + w\xi_z$$

$$\tilde{v} = u\eta_x + v\eta_y + w\eta_z$$

$$\tilde{w} = u\zeta_x + v\zeta_y + w\zeta_z$$

where J is the Jacobian of the transformation and ξ_x, η_x ... etc. are identified with the grid metrics of the transformation. In practice, the terms $J\xi_x, J\eta_x$ ... etc., required in the flux terms, are identified with the projected areas of each cell face. They are computed by taking the cross product of the two vectors joining opposite corners of each cell face in the Cartesian coordinate system. The physical variables required in the transformed flux evaluation may be averaged on each cell face through the four nodal values associated with each face.

The above scheme reduces to a second order accurate, nondissipative central difference approximation to the Euler equations on sufficiently smooth Cartesian meshes. A central difference scheme permits odd-even decoupling at adjacent nodes which may lead to oscillatory solutions. To prevent this "unphysical" phenomena from occurring, a dissipation term is added to the system of equations such that the system now becomes,

$$\frac{d}{dt^*}(V_{ijk}\mathbf{w}) + \mathbf{P}\left[Q_{ijk}(\mathbf{w}) - D_{ijk}(\mathbf{w})\right] = 0. \quad (4)$$

For the present problem a third order background dissipation term is added. The dissipative term is constructed in such a manner that the conservation form of the system of equations is preserved. The basic scheme for the dissipation is,

$$D_{ijk}(\mathbf{w}) = D_x + D_y + D_z \quad (5)$$

where

$$D_{x_{ijk}} = d_{x_{i+1,j,k}} - d_{x_{i,j,k}}$$

and

$$d_{x_{i,j,k}} = \alpha\delta_x^2(\mathbf{w}_{i+1,j,k} - \mathbf{w}_{i,j,k}). \quad (6)$$

Similar expressions may be written for the y and z directions with δ_x^2, δ_y^2 and δ_z^2 representing second difference central operators.

In equation 6, the dissipation coefficient α is a scaling factor, proportional to the local wave speed. The actual form for the coefficient is based on the spectral radius of the system and is given in the x direction as,

$$\alpha = \epsilon(|\tilde{u}| + \Gamma(S_x^2 + S_y^2 + S_z^2)^{1/2})$$

where $\tilde{u}$ is the contravariant velocity component and S_x, S_y and S_z are the directed face areas. Similar dissipation coefficients are used for the y and z components in equation 5. The ϵ term is used to manually adjust the amount of dissipation and is small, usually around 1/256.

Equation 4 is integrated in time by an explicit multistage scheme. For each bulk flow time step, the mesh, and thus V_{ijk}, is independent of time. Hence equation 4 can be written as

$$\frac{d\mathbf{w}_{ijk}}{dt^*} + R_{ijk}(\mathbf{w}) = 0, \quad (7)$$

where

$$R_{ijk}(\mathbf{w}) = \frac{1}{V_{ijk}}\mathbf{P}(Q_{ijk} - D_{ijk}).$$

The actual time step Δt is limited by the Courant number (CFL). This basically states that the fastest waves in the system may not be allowed to propagate farther than the smallest mesh spacing over the course of a time step. In this work local time stepping was used such that regions

of large mesh spacing are permitted to have relatively larger time steps than regions of small mesh spacing. Of course the system wave speeds vary locally and must be taken into account as well. The final, local, time step was thus computed as,

$$\Delta t^*_{ijk} = \frac{(CFL)V_{ijk}}{\lambda_{ijk}}$$

where λ_{ijk} is the sum of the spectral radii in the x, y and z directions. Clearly, it may be seen that in regions of small mesh spacing and/or regions of high characteristic wave velocities, the time step will be smaller than in other regions.

The allowable Courant number may be made larger by smoothing the residuals at each stage. This is done in the following product form in three dimensions,

$$(1 - \epsilon_x\delta_x^2)(1 - \epsilon_y\delta_y^2)(1 - \epsilon_z\delta_z^2)\bar{R} = R.$$

where ϵ_x, ϵ_y and ϵ_z are smoothing coefficients and the $\delta^2_{x,y,z}$ are central difference operators. Thus each residual is replaced by an average of itself and the neighboring residuals.

An effective method to accelerate convergence is the multigrid method. This is accomplished through tracking the evolution of the system of equations on successively coarser meshes such that larger time steps may be used to more rapidly reduce the system residuals. Auxiliary meshes are introduced by doubling the mesh spacing and values of the flow variables are transferred to a coarser grid by the rule,

$$\mathbf{w}^{(0)}_{2h} = \sum V_h \mathbf{w}_h / V_{2h},$$

where the subscripts denote values of the mesh spacing parameter (ie. h is the finest grid, $2h$, $4h$, ... etc. are successively coarser grids). In three dimensions the sum is over the eight cells surrounding any particular mesh point; these eight cells then become a new coarse grid cell. A forcing term is then defined as

$$\mathbf{P}_{2h} = \sum R_h(\mathbf{w}_h) - R_{2h}(\mathbf{w}^{(0)}_{2h}),$$

where R is the residual of the difference scheme. To update the solution on the coarse grid the multistage scheme is reformulated as

$$\begin{aligned}
\mathbf{w}^{(1)}_{2h} &= \mathbf{w}^{(0)}_{2h} - \alpha_1 \Delta t^*(R^{(0)}_{2h} + P_{2h}) \\
&\cdots \\
\mathbf{w}^{(q+1)}_{2h} &= \mathbf{w}^{(0)}_{2h} - \alpha_q \Delta t^*(R^{(q)}_{2h} + P_{2h}) \\
&\cdots
\end{aligned}$$

where $R^{(q)}$ is the residual of the q^{th} stage. In the first stage, the addition of P_{2h} cancels $R_{2h}(\mathbf{w}^{(0)})$ and replaces it by $\sum R_h(\mathbf{w}_h)$, with the result that the evolution on the coarse grid is driven by the residual on the fine grid. The result $\mathbf{w}^{(m)}_{2h}$ now provides the initial data for the next mesh $\mathbf{w}^{(0)}_{4h}$ and so on. Once the last grid has has been reached the accumulated correction must be passed back through successively finer grids. Assuming a three grid scheme, let $\mathbf{w}^{(+)}_{4h}$ represent the final value of $\mathbf{w}_{4h}$. Then the correction for the next finer mesh will be

$$\mathbf{w}^{(+)}_{2h} = \mathbf{w}^{(m)}_{2h} + I_{2h,4h}(\mathbf{w}^{(+)}_{4h} - \mathbf{w}^{(0)}_{4h}),$$

where $I_{a,b}$ is an interpolation operator from the coarse grid to the next finer grid. The final result on the fine mesh is obtained in the same manner, ie.

$$\mathbf{w}^{(+)}_{h} = \mathbf{w}^{(m)}_{h} + I_{h,2h}(\mathbf{w}^{(+)}_{2h} - \mathbf{w}^{(0)}_{2h}).$$

The process may be performed on any number of successively coarser grids. The only restriction in the present work being use of a structured grid whereby elements of the coarsest mesh do not overlap the ship hull. A 3-level "W-cycle" is used in the present work for each time step [12].

3.2 Free Surface Solution

Both a kinematic and dynamic boundary condition must be imposed at the free surface. For the fully nonlinear condition, the free surface must move with the flow (ie. up and down corresponding to the wave height and location) and the boundary conditions are applied on the distorted free surface. The most successful method found in this work to couple the free surface and bulk flow solvers is described as follows. First, equation 2 can be cast in a form more amenable to numerical computations by introducing a curvilinear coordinate system that transforms the curved free surface $\beta(x, y)$ into computational coordinates $\beta(\xi, \eta)$. This results in the following transformed kinematic condition,

$$\beta_{t^*} + U\beta_\xi + V\beta_\eta = w \qquad (8)$$

where U and V are contravariant velocity components given by

$$U = u\xi_x + v\xi_y,$$

$$V = u\eta_x + v\eta_y.$$

The free surface kinematic equation may now be expressed as

$$\frac{d\beta_{ij}}{dt^*} + Q_{ij}(\beta) = 0,$$

where $Q_{ij}(\beta)$ consists of the collection of velocity and spacial gradient terms which result from the discretization of equation 8. Note that this is not the result of a volume integration and thus the volume (or actually area) term does not appear in the residual as in the FVM formulation. Throughout the interior of the (x, y) plane, all derivatives are computed using the second order centered difference stencil in computational coordinates ξ and η. On the boundary a second order centered stencil is used along the boundary tangent and a first order one sided difference stencil is used in the boundary normal direction.

As was necessary in the FVM formulation for the bulk flow, background dissipation must be added to prevent decoupling of the solution. The method used to compute the dissipation terms borrows from a two dimensional FVM formulation and appears as follows:

$$D_{ij} = D_x + D_y$$

where

$$D_{x_{ij}} = d_{x_{i+1,j}} - d_{x_{i,j}}$$

and

$$d_{x_{i,j}} = \alpha\delta_x^2(\beta_{i+1,j} - \beta_{i,j}).$$

The expression for α may be written as

$$\alpha = \epsilon(|U_{i+1,j}| + |U_{i,j}|)$$

where $U_{i,j}$ is the unscaled contravariant velocity component defined by

$$U = uy_\eta - vx_\eta.$$

Hence the system of equations for the free surface is expressed as

$$\frac{d\beta_{ij}}{dt^*} + R_{ij}(\beta) = 0,$$

where

$$R_{ij} = Q_{ij} - D_{ij}/A_{ij}$$

and A_{ij} is the area of the cells surrounding node ij. The same method of update used in equations 7 is used here. Once the free surface update is accomplished the pressure is adjusted on the free surface such that,

$$\psi^{(n+1)} = \beta^{(n+1)}F_T{}^{-2}.$$

The coupling between the free surface and the bulk flow is established by computing a solution at a time step for the bulk flow and then using the bulk flow as a boundary condition for the free surface. The free surface elevation is updated and its present values are used as a boundary condition for the pressure on the bulk flow. This iterative process repeats until some measure of convergence is attained; usually steady state wave profile and/or wave resistance coefficient.

An additional point in the scheme concerns tangency of the flow on the free surface. Since the free surface is considered a material surface, the flow must be tangent. In this work, the flow is allowed to *leak* through the surface while marching towards steady state. It is this leakage that, in effect, drives the evolution equation. Consider that during the iteration, the vertical velocity component w is positive (cf. equation 2 or 8). This will, provided other terms are small, force β^{n+1} to be greater than β^n. Thus, when the time step is complete ψ is adjusted such that $\psi^{n+1} > \psi^n$ as well. Since the free surface has been effectively moved farther away from the original datum, or undisturbed upstream elevation, and the pressure correspondingly increased, then the velocity component w (or better still $\mathbf{q}\cdot\mathbf{n}$ where $\mathbf{n} = \frac{\nabla F}{|\nabla F|}$ and $F = z - \beta(x, y)$) will be reduced. This results in a smaller $\Delta\beta$ for the next time step. The same is true for negative velocity as well, ie. mass leakage into the system rather than out. Only when steady state has been reached is the mass flux through the surface zero and tangency enforced. In fact, the residual flux leakage could be used in addition to drag components and pressure residuals to define the steady state condition.

4 Results for Wigley Parabolic Hull

Figure 2 shows the computed wave profiles, from bow to stern along the hull, compared with experiments conducted at the University of Tokyo [14]. The agreement with experiment is extremely favorable. Amplitudes at all peaks and troughs as well as wavelength are in excellent agreement with experiment. The only discrepancy noted is near the stern where separation and/or eddy losses, albeit small, may be present in experiments.

Figure 3 shows the computed wave drag as the

simulation proceeds. The wave drag was computed by integrating the component of the static pressure, in the longitudinal direction, over the wetted surface of the hull. For each Froude number, the computed wave drag overpredicts the experimentally determined wave drag by about the same amount. This overprediction most likely arises from the comparison of viscous experiments with a purely inviscid numerical scheme. There is also the possibility of some error in the numerical integration of the pressure field on the hull surface; however, this is considered small if not negligible. It remains to incorporate the viscous terms and make a more meaningful comparison of not only the wave drag but the frictional drag as well. Aside from the overprediction, the computed steady state wave drag follows the general trend predicted by the Michell theory, ie. interference between bow and stern wakes lead to oscillations in a wave drag versus ship velocity curve [16].

Figures 4 and 5 show perspective views of the final distorted grid mesh and the resulting pressure field (ψ) on the hull for $Fr = 0.2670$. The divergent and transverse wave systems, originating from both bow and stern, are in excellent agreement with the geometry predicted by the linear Kelvin theory [17], ie. the waves are confined by straight line sectors of ± 19.46 degrees.

Figures 6 and 7 show convergence history of the pressure residual and computed free surface Bernoulli constant, for various Froude numbers, as the simulation proceeds. The pressure residual, computed by taking the root mean square of $\frac{d\psi}{dt}$, is important since it affords a measure of the error in divergence of mass, or continuity, through the first of equations 3; ie.,

$$\frac{1}{\Gamma^2}\frac{\partial \psi}{\partial t^*} + \nabla \cdot \mathbf{q} = 0.$$

As shown in figure 6, the computed residual is small thus implying that equation 1 is closely satisfied. It is probably the "leap frog" nature of the iterative scheme that prevents the error from becoming smaller; the bulk flow solution and free surface solution continually adjust each other leading to minute changes in free surface height ($\Delta\beta \approx 10^{-6}$), whence, minute changes in $\Delta\psi$. The Bernoulli constant B is computed by summing all the free surface nodal values of

$$B_{ij} = \frac{1}{2}(\mathbf{q}\cdot\mathbf{q} - 1) + \psi$$

and dividing by the number of free surface nodes. This represents another measure of convergence of the scheme since it is fairly constant and close to the expected value of zero.

A final comment in regards to convergence and accuracy is that the information desired from the simulation, usually wave drag, can be obtained in approximately 400 multigrid cycles. One can see from figures 3, 6 and 7 that the wave drag, pressure residual and Bernoulli constant change little beyond this point. What will change is the continuing evolution of the downstream wave profile; but this has little effect on the computed drag once the profile near the ship hull has been established. The results presented herein use 700 cycles only to show the long time convergence and stability properties of the scheme.

5 Conclusions

The objective of the present work was to develop an efficient method for solving the incompressible flow problem, about arbitrary ship hulls, in conjunction with a free surface. As mentioned in the Introduction, this required two areas of work. First, the free surface location must be part of the solution since it is unknown *a priori*. Secondly, the incompressibility constraint must be enforced to facilitate calculation of the proper free surface location and evaluation of the pressure field on the hull. The results for the Wigley hull suggest that the objective has been reached and the resulting computer code has been validated, at least for the range of test cases examined. Excellent agreement between experiment and numerical simulation has been obtained in regards to wave elevation. In addition, the computed wave drag, derived from integrating the hull pressure field, is in good agreement for the Froude numbers examined.

Perhaps the most pressing area requiring additional work is the inclusion of viscous fluxes and a turbulence model. Stemming from the ability to compute the frictional drag, this may also facilitate more accurate comparisons of the wave drag with experimental measurement. A second area of work is the simulation of an actual sailing yacht with attached keel at an angle of attack.

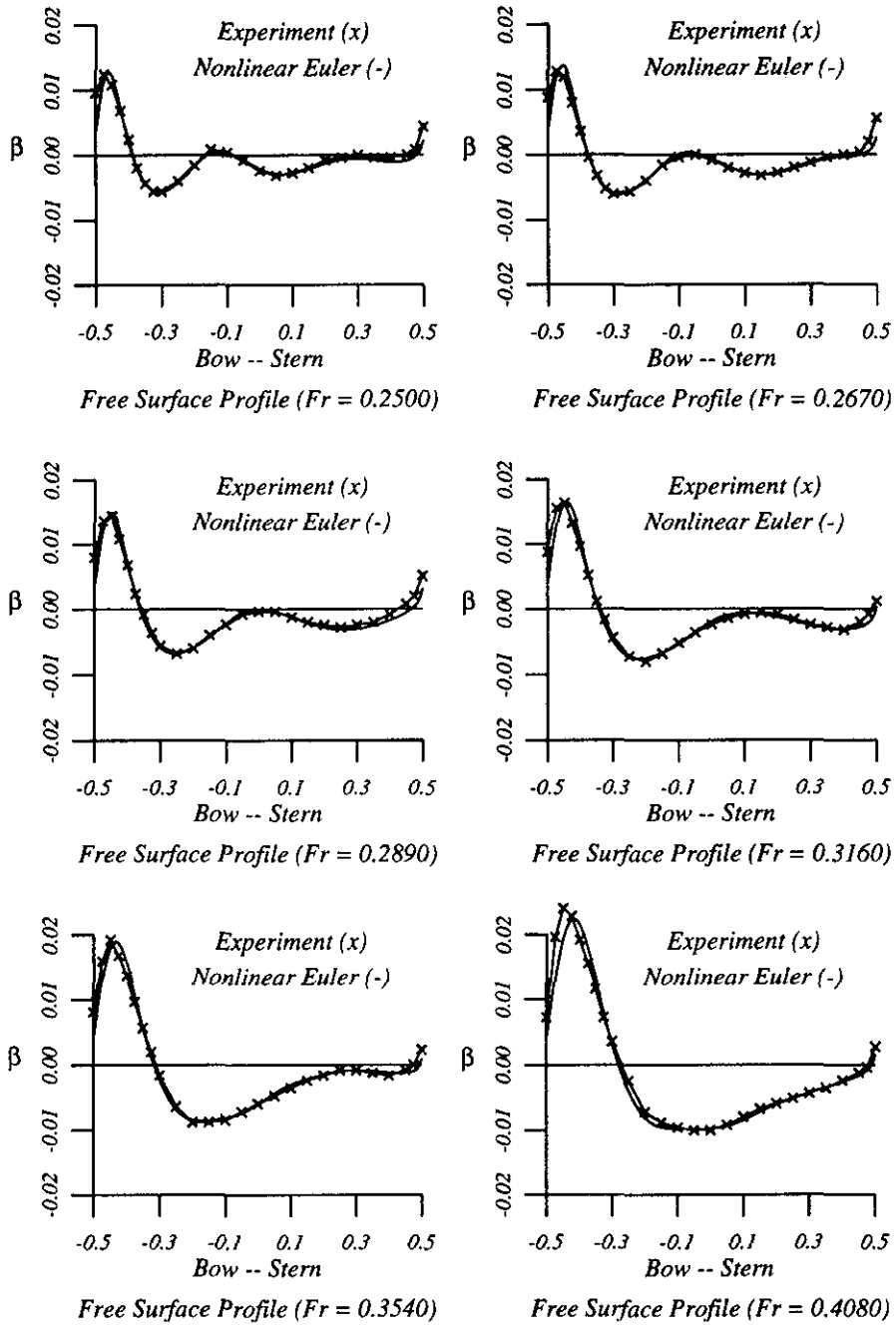

Figure 2: Wigley Parabolic Hull Wave Profiles

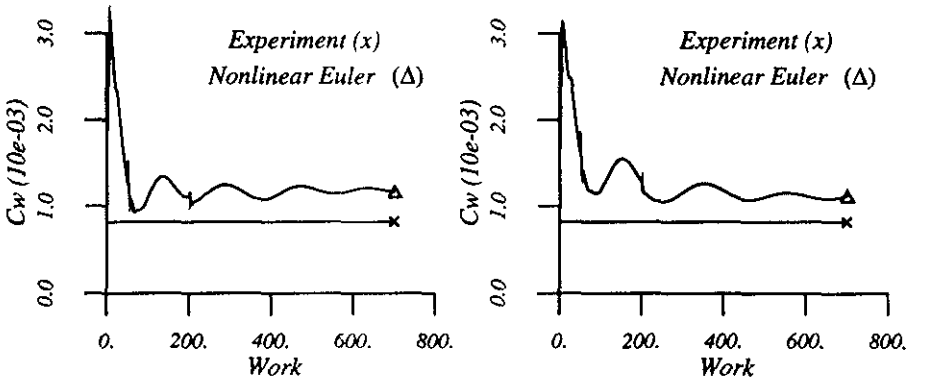

Wave Resistance vs. Work (Fr = 0.2500) Wave Resistance vs. Work (Fr = 0.2670,

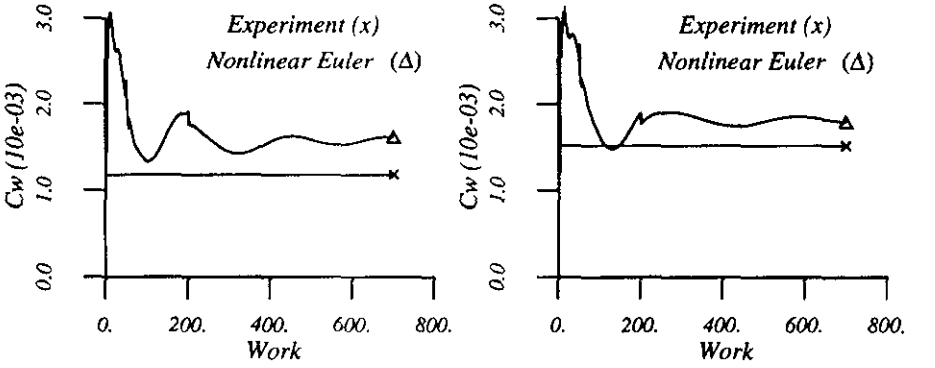

Wave Resistance vs. Work (Fr = 0.2890) Wave Resistance vs. Work (Fr = 0.3160,

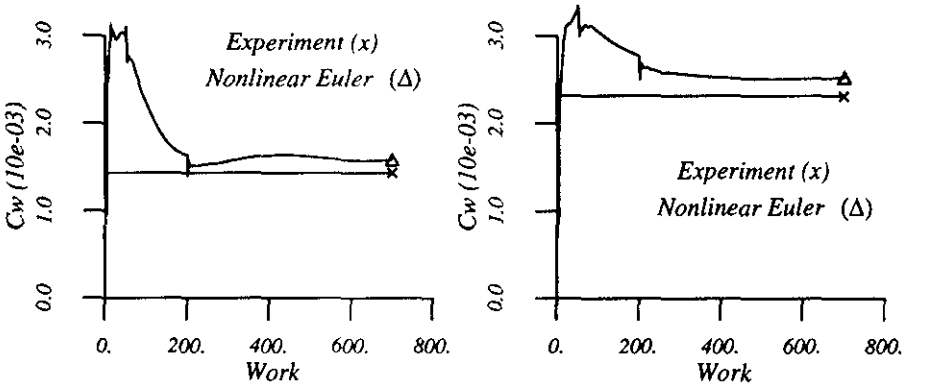

Wave Resistance vs. Work (Fr = 0.3540) Wave Resistance vs. Work (Fr = 0.4080,

Figure 3: Wave Resistance History

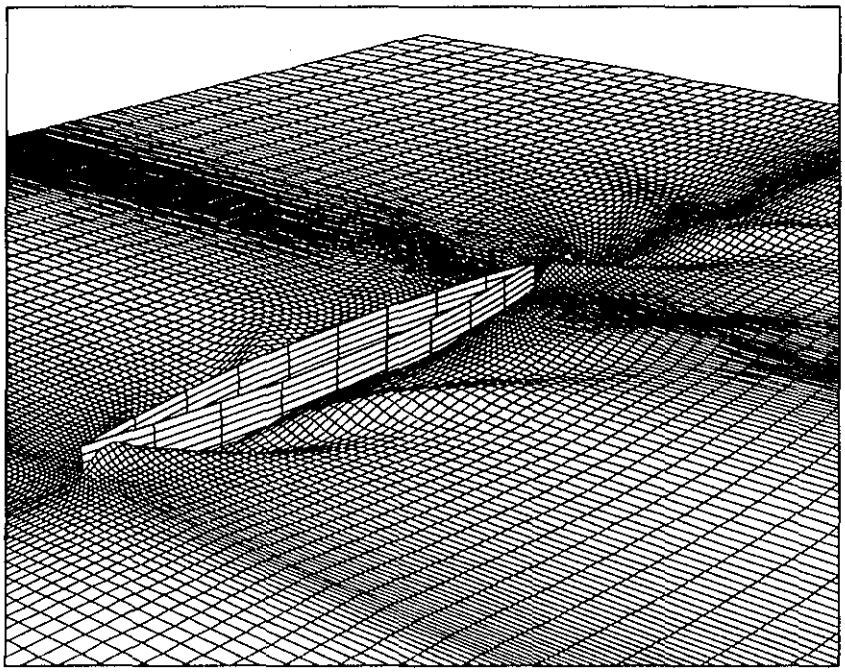

Figure 4: Perspective View of Wave Elevation, Fr=0.2670
(Wave elevation multiplied three times.)

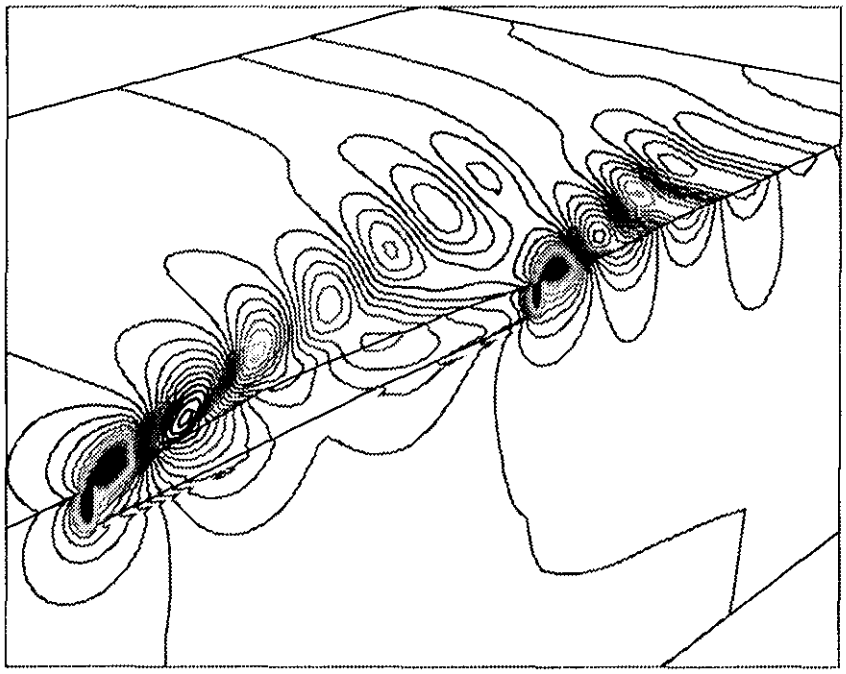

Figure 5: Perspective View of Pressure Contours, Fr=0.2670
(Starboard Side)

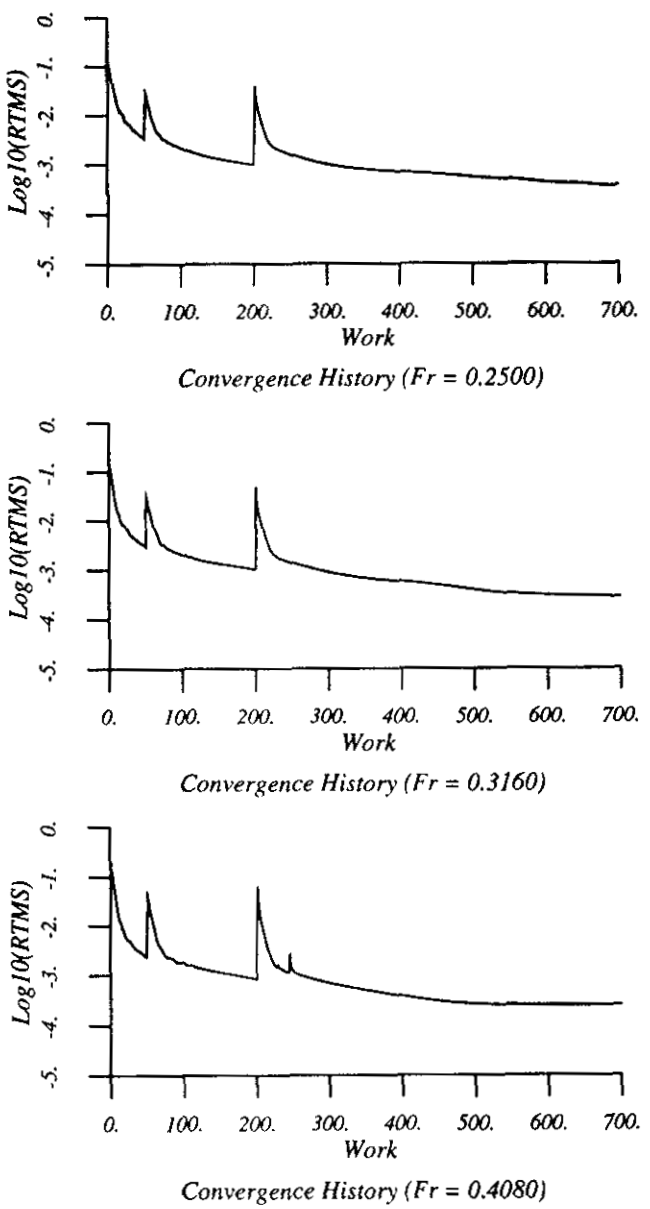

Figure 6: Convergence History

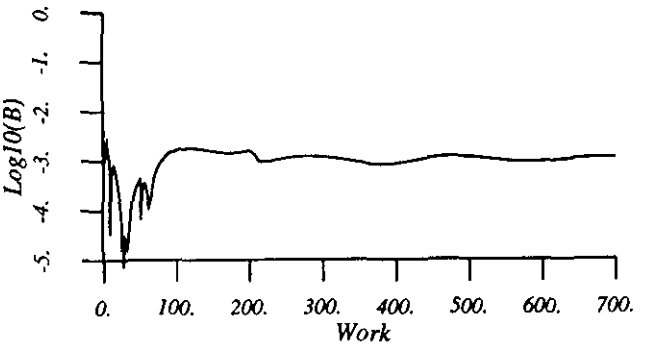

Computed Bernoulli Constant (Fr = 0.2500)

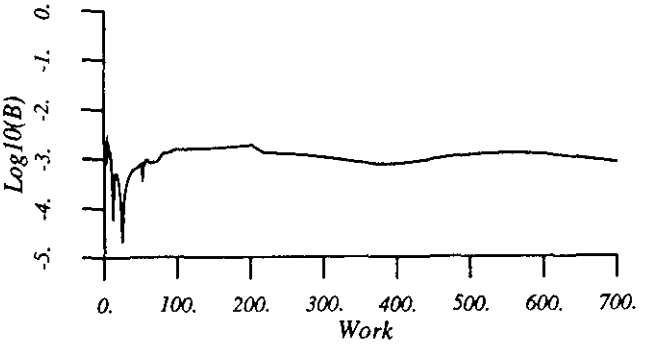

Computed Bernoulli Constant (Fr = 0.3160)

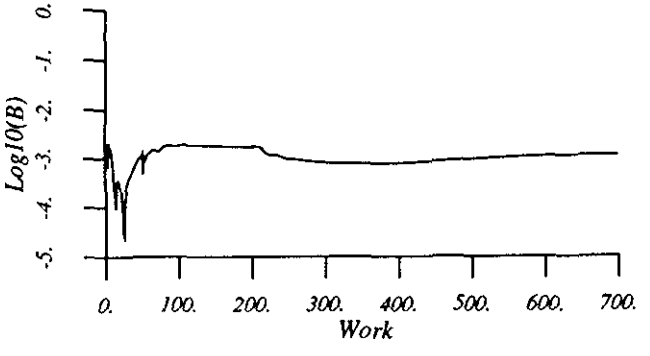

Computed Bernoulli Constant (Fr = 0.4080)

Figure 7: Computed Bernoulli Constant

References

[1] Jameson,A., Baker,T., and Weatherill,N., "Calculation of Inviscid Transonic Flow Over a Complete Aircraft", *AIAA Paper 86-0103, AIAA 24th Aerospace Sciences Meeting,* Reno, January 1986.

[2] Hino,T., "Computation of Free Surface Flow Around an Advancing Ship by the Navier-Stokes Equations", *Proceedings, Fifth International Conference on Numerical Ship Hydrodynamics,* pp. 103-117, 1989.

[3] Miyata,H., Toru,S., and Baba,N., "Difference Solution of a Viscous Flow with Free-Surface Wave about an Advancing Ship", *Journal of Computational Physics,* v. 72, pp. 393-421, 1987.

[4] Tahara,Y., Stern,F., and Rosen,B., "An Interactive Approach for Calculating Ship Boundary Layers and Wakes for Nonzero Froude Number", *Journal of Computational Physics,* v. 98, pp. 33-53, 1992.

[5] Chorin,A., "A Numerical Method for Solving Incompressible Viscous Flow Problems", *Journal of Computational Physics,* v. 2, pp. 12-26, 1967.

[6] Rizzi,A., and Eriksson,L., "Computation of Inviscid Incompressible Flow with Rotation", *Journal of Fluid Mechanics,* v. 153, pp. 275-312, 1985.

[7] Dreyer,J., "Finite Volume Solutions to the Unsteady Incompressible Euler Equations on Unstructured Triangular Meshes", M.S. Thesis, MAE Dept., Princeton University, 1990.

[8] Kodama,Y., "Grid Generation and Flow Computation for Practical Ship Hull Forms and Propellers Using the Geometrical Method and the IAF Scheme", *Proceedings, Fifth International Conference on Numerical Ship Hydrodynamics,* pp. 71-85, 1989.

[9] Turkel,E., "Preconditioned Methods for Solving the Incompressible and Low Speed Compressible Equations", ICASE Report 86-14, 1986.

[10] Jameson,A., "Solution of the Euler Equations for Two Dimensional Transonic Flow by a Multigrid Method", *Applied Math. and Computation,* v. 13, pp. 327-356, 1983.

[11] Jameson, A., "Computational Transonics", *Comm. Pure Appl. Math.,* v. 41, pp. 507-549, 1988.

[12] Jameson,A., "A Vertex Based Multigrid Algorithm For Three Dimensional Compressible Flow Calculations", *ASME Symposium on Numerical Methods for Compressible Flows,* Annaheim, December 1986.

[13] Farmer,J., "A Finite Volume Multigrid Solution to the Three Dimensional Nonlinear Ship Wave Problem", Ph.D. Thesis, Princeton University, January 1993.

[14] "Cooperative Experiments on Wigley Parabolic Models in Japan", *17th ITTC Resistance Committee Report,* 2nd ed., 1983.

[15] Orlanski,I., "A Simple Boundary Condition for Unbounded Hyperbolic Flows", *Journal of Computational Physics,* v. 21, 1976.

[16] Wehausen,J.V., "The Wave Resistance of Ships", *Advances in Applied Mechanics,* v. 13, pp. 93-245, 1973.

[17] Stoker,J.J., *Water Waves,* Interscience Publishers, Inc. New York, 1957.